European Rotorcraft Forum

WIND TUNNEL INVESTIGATION OF A HELICOPTER MODEL IN SHIPBOARD OPERATIONS

N. Taymourtash*, D. Zagaglia, A. Zanotti, G. Gibertini, G. Quaranta
Politecnico di Milano - Dipartimento di Scienze e Tecnologie Aerospaziali
Campus Bovisa, Via La Masa 34, 20156 Milano, Italy
* Politecnico di Milano and University of Glasgow, e–mail: neda.taymourtash@polimi.it

Abstract
The paper presents the wind tunnel simulation of a helicopter model in shipboard operations. The test rig consists of a scaled helicopter model and a simplified ship model, based on the geometry of the Simple Frigate Shape 1. In the first phase of the experiment, pressure and Particle Image Velocimetry survey of the flow field on the flight deck were performed without the presence of the helicopter, to study the flow features on the ship deck, for several wind conditions obtained modifying the wind speed and direction. The influence of Atmospheric Boundary Layer was investigated as well. Then, the rotorcraft was positioned in a series of points representative of both a typical fore-aft landing trajectory toward the deck, and a vertical descent on the deck. Loads generated by the rotor were monitored by means of a six-axis load cell. Particle Image Velocimetry of the ship wake and of the helicopter inflow were carried out in order to have a better understanding of how the interacting flow fields affected the helicopter performance. The test showed a significant effect of the mutual aerodynamic influence between the helicopter and the ship model and a limited effect of the Atmospheric Boundary Layer.

Keywords: Rotorcraft, Aerodynamics, Vortex Interaction, Particle Image Velocimetry (PIV), Shipboard Operations, Wind Tunnel.

NOMENCLATURE

A	Rotor disc area
c	Blade chord
c_P	Pressure coefficient, $2(P-P_\infty)/(\rho U_\infty^2)$
c_T	Thrust coefficient, $T/\left(\rho\Omega^2R^2A\right)$
c_M	Moment coefficient, $M/\left(\rho\Omega^2R^2AR\right)$
ABL	Athmospheric Boundary Layer
GVPM	Galleria del Vento Politecnico di Milano
M_{TIP}	Mach Number at blade tip
R	Rotor disc radius
Re_{TIP}	Reynolds Number at blade tip, $\Omega Rc/\nu$
V_{IND}	Rotor induced velocity
U_∞	Wind velocity
β	Ship sideslip angle
μ	Advance ratio, $U_\infty/(\Omega R)$
Ω	Rotor rotational frequency
ABL	Athmospheric Boundary Layer
GVPM	Galleria del Vento Politecnico di Milano
IGE	In Ground Effect condition
OGE	Out of Ground Effect condition
PIV	Particle Image Velocimetry

1. INTRODUCTION

Helicopters, owing to their ability of managing hovering flight, are regularly required to perform challenging missions in which they have close interaction with obstacles in the surrounding environment, such as search and rescue missions, urban transport, medical emergency services and offshore operations. The aerodynamic interaction could be even more complicated when the environment is moving by itself, like operation on moving decks or manoeuvring in gusty wind condition. The complex flow-field developed in these situations, due to large vortical structures detached by the hull or the deck, negatively affects the performance and handling qualities of the helicopter and may endanger the safety of flight, since the pilot workload increases significantly.

When the wind influence is taken into account together with ship motion, it is possible to define a

dynamic-interface safe operating envelope which is unique for every helicopter/ship combination. Analysis of safety operating limits for such demanding tasks is inevitable and can be done either through a series of flight tests at sea or development of Dynamic Interface Simulation(DIS). The flight tests are typically high costs and in general difficult to be performed since the proper weather conditions must be met. Consequrently, the construction of the dynamic-interface requires a large amount of engineering/pilot judgment and, unless the critical conditions are flown, it is usually very conservative[1].

The development of Dynamic Interface Simulation can remarkably reduce the cost and hazard of time-consuming at-sea test campaigns[2]. However, the full CFD simulation of the ship to catch the interactive flowfield is computationally expensive, and it is often not fully representative of the mutual influence between the ship wake and the helicopter wake and the correctness of the overall solution obtained by the principle of superposition is highly questionable, as shown in Ref[3].

A better understanding of the airwake generated by helicopter-ship interaction is of great importance and it has been the major focus of extensive numerical and experimental works for over a decade, as documented by Zan[4]. A better understanding of flow conditions could lead to the development of a more accurate simulation environment for such demanding operations, allowing for significant reduction of the number of tests at-sea and reducing the uncertainties. At the same time this improved simulation environment may be used to improve pilot training. All those elements will increase safety of rotorcraft operations, which is the objective of the NITROS project[5]. The present work falls within the framework of this project.

One of the first experimental investigations in this field was done by Zan[4] at the Aerodynamic Laboratory of the National Research Council of Canada. The experiments were conducted at a geometric scale of 1:50 of the Canadian Patrol Frigate and CH-124 Sea King. Initial experiment presented the measurements of the time averaged rotor thrust coefficients for the rotor immersed in CPF airwake[6]. This study has demonstrated that the reduced inflow on the rotor, due to ship airwake, can significantly decrease rotor thrust up to 15 percent. The results also confirmed the strong influence of wind speed and direction on the airwake and, consequently, on the rotor thrust and operational envelope. Another experiment was conducted using the same ship model, to measure unsteady loads acting on the rotor-less helicopter fuselage. A reasonable correlation was found between root-mean-square (RMS) loading levels and pilot workload obtained from flight test[7]. The additional influence of the rotor downwash on the unsteady loading of the fuselage was also studied and compared using these rotor-less cases[8].

Kääriä et. al.[9] proposed a different test setup to characterize the aerodynamic loading of a 1:54 model-scale helicopter immersed in the airwake of a generic frigate ship. The experiments were conducted in a water tunnel using a specially designed Airwake Dynamometer (AirDyn) identifying specific time-averaged and unsteady loading characteristics caused by the severe spatial and temporal velocity gradients in the airwake. The setup was used also to investigate the potential benefits of aerodynamic modifications to the ship geometry[10]. They studied various modifications and concluded that all of them are effective in reducing the RMS of forces and moments. In particular, the promising design concepts were a side-flap and notch modification which both showed consistent improvements of 25-50 percent in RMS of loads.

To identify the rotor downwash and ship airwake coupling, flow visualization techniques have been utilized as well, providing information on development of the interacting flowfield during the landing maneuver. Landman et al.[11,12] conducted an experiment exploiting Particle Image Velocimetry(PIV) with the ship and rotor in isolation and then the combined case in order to investigate the superimposed velocity field and recirculation region. Furthermore, an extensive rotor thrust survey was conducted highlighting the significant variations close to the landing deck.

In addition to shipboard operation, there are some studies regarding the interaction of rotorcraft with simple shape obstacles like building. For instance, Quinliven et. al.[13] evaluated the effects of the aerodynamic wake from a large upstream object, such as a building, on a rotorcraft operating in proximity to that object. In this experiment, smoke visualization was used with high intensity light in order to visualize the flow field. Also, induced velocities were measured using the pressure probes distributed spanwise along each blades. The results showed that upwind building presence tended to decrease the induced velocities at the leading edge of the rotor disc, which is consistent with the presence of a recirculation region between the rotor and the building.

A series of experiments has been performed by Zagaglia et. al.[14], in which a thoroughly investigation of the rotorcraft interaction with a ground obstacle was tested. Initially a series of tests to replicate different hovering conditions in absence of the external wind were performed[14]. Then, the performance of the rotor was assessed in moderate windy

conditions for several positions with respect to the obstacle[15]. The helicopter model, including a four-bladed rotor and fuselage, was positioned in different points relative to a simplified obstacle with a parallelpiped shape. The forces and moments acting on the rotor were measured with a six component balance nested inside the fuselage. PIV survey was used to investigate the details of the interacting flow field. The results showed a very strong variations in thrust and in-plane hub moments when the helicopter enters in the obstacle wake[15].

The objective of this research is to improve the capability to estimate the flowfield on this higly interactive condition. For this reason, experimental tests are planned together with the possibility to exploit this experiment to improve the fidelity of flight simulations, including the possibility to use the results of wind tunnel experiments directly as an element of a hardware-in-the-loop experiment[16].

The main objective of this paper is the experimental investigation of the interacting flow field between helicopter and ship airwake while approaching the flight deck. Taking advantage of the large test chamber (section 13.84 m x 3.84 m) of the Wind Tunnel of Politecnico di Milano (GVPM), the geometric scale of 1:12.5 of Simple Frigate Shape 1 (SFS1) was considered, which resulted in a quite higher Reynolds Number compared with similar investigations performed in the past[6,9]. The paper starts with the description of the experimental setup, describing both models, the scaling parameters, the measures performed and the description of the method to reproduce the Atmospheric Boundary Layer (ABL) in the test chamber. Then, the description of the test points and conditions is given, presenting the trajectories considered representative of a typical approach to the flight deck along the centerline followed by an oblique path toward the landing spot, and of a vertical descent trajectory. Finally, some conclusions are drawn.

2. EXPERIMENTAL SETUP

The test rig, as shown in Figure 1, consists of a helicopter model and a simplified ship model, to which the bow has been cut. The helicopter model is held by a horizontal strut fixed to a system of two motorised orthogonal sliding guides which is able to change the relative position of the helicopter with respect to the ship in both vertical and longitudinal directions. A fixed coordinate system is defined to introduce the test points, which represents the position of the rotor hub center with respect to the ship. The XZ plane of this reference frame is aligned with the longitudinal plane of the ship that contains the

Figure 1: The test rig mounted inside the GVPM.

roll axis and the Y axis is aligned with the pitch axis of the ship, with the origin on the floor of the wind tunnel and the end of the stern, see Figure 2.

2.1. Ship Model

Considering the ship landing maneuver as one of the most challenging missions in terms of aerodynamic interaction, the shape of the obstacle is representative of a ship geometry. However, the details of the ship superstructure were not considered relevant in this research. So, Simple Frigate Shape 1 was selected which is a highly simplified but representative ship geometry, developed as a part of an international collaboration in which Canada, Australia, UK and USA evaluated the ability of CFD codes to simulate complex airwakes[17]. The model, as shown in Figure 2, is a rectangular prism with a step on its rear and another prism on top which is acting like ship superstructure. The SFS1 was scaled down with a geometric factor of 12.5 in order to have enough space on the flight deck for landing of the helicopter model. The flight deck and hangar wall were equipped with 66 and 30 pressure taps respectively. Furthermore, five high sensitivity Kulite transducers, with sampling frequency of 25000 Hz, were placed along the longitudinal centerline of the flight deck in order to measure the unsteady pressure. The layout of the pressure taps and Kulite transducers is shown in Figure 2. In order to investigate the effect of wind direction, the ship model was placed on the large turntable of the test section. With the landing point placed on the center of the turntable, the ship can be rotated to both sides, while the landing point remains fixed with respect to the boundaries of the test section.

2.2. Helicopter Model

Helicopter model consists of a fuselage and a rotor which has four untwisted and untapered rectangu-

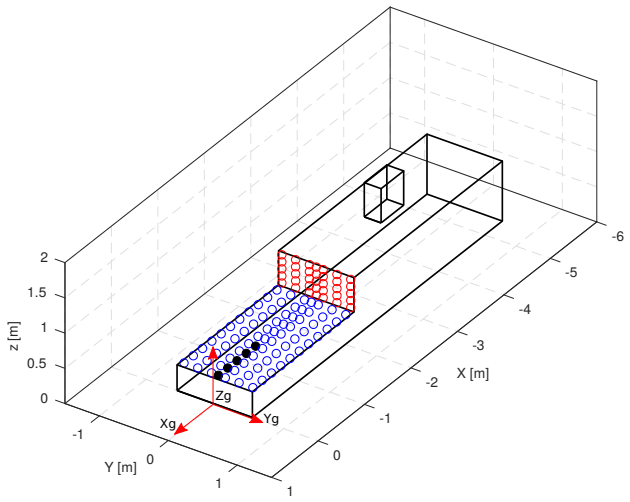

Figure 2: Scale model of SFS1 equipped with pressure taps and Kulite transducers.

lar blades with NACA0012 airfoil. Since no swashplate was implemented in the current version of the model, the rotor could not be trimmed and the blade pitch angle was fixed to 10°. The rotational speed of the rotor was maintained in all tests by means of a brush-less low-voltage electrical motor with an electric controller. A Hall effect sensor with sampling frequency of one per revolution was implemented which acts as the feedback signal for RPM control. The loads acting on the rotor were measured using a six-components balance nested inside the fuselage with the sampling frequency of 100 hz. The adopted load cell allowed force measurements accurate up to 0.4% of the out of ground effect (OGE) thrust values, while moment measurements were accurate up to 0.48% of OGE torque.

2.3. Scaling Parameters

The main scaling objective in this experiment is to correctly replicate the advance ratio of the full scale model which ensuring also the similarity of the reduced frequency. The helicopter model is not representative of an exact aircraft but could be taken as representative of a Bo-105-like helicopter. In fact, in this case the geometric scale is equal to 1:13.1. Advance ratio scaling relates three parameters of the test, including: rotational frequency of the rotor, geometric scale and free stream velocity:

$$(1) \quad \frac{\mu_1}{\mu_2} = \frac{U_{\infty_1}}{U_{\infty_2}} \frac{R_2}{R_1} \frac{\Omega_2}{\Omega 1}$$

The rotational frequency of the rotor was selected high enough in order to increase the Reynolds number and Mach number, while reaching the desired advance ratio within the limits of free stream velocity of the wind tunnel test section. Moreover, to avoid issues with vibratory loads caused by high rotational frequency it was decided to limit the angular speed. Consequently, a velocity scale of 1:2.16 was set, leading to frequency scale of 6.06:1 that were maintained during all tests. The parameters of the scaled and wind tunnel models are summarized in Table 1.

Table 1: Parameters of Wind Tunnel (WT) model and full scale model.

Characteristic	WT model	Full scale
Number of Blades	4	4
Rotor Radius(m)	0.375	4.9
Angular Velocity(rad/s)	270	44.4
Blade Chord(m)	0.032	0.27
Free Stream Velocity(m/s)	4.76	10.29
Advanced Ratio	0.047	0.047
Tip Mach Number	0.3	0.63
Tip Reynolds Number	$2.2e5$	$3.9e6$

It is worth mentioning that the ship-based Reynolds number of about 11,000 is considered to be adequate for sharp-edged models[18]. Considering the selected free stream velocity in this experiment, the ship Reynolds number, defined based on the beam length, is about 350,000 which is well above than minimum required number.

2.4. PIV Setup

The PIV system comprised a Litron NANO-L-200-15 Nd:Yag double-pulse laser with an output energy of 200 mJ and wavelength of 532 nm, and one Imperx ICL-B1921M CCD cameras with a 12-bit, 1952×1112 pixel array. The laser was positioned on a suitable strut downstream of the ship model so that the laser sheet was aligned with the XZ plane and could span the whole shipdeck. The camera line of sight was positioned perpendicular to the laser sheet. In order to achieve a better resolution of the image pairs, the measurement area comprised multiple adjacent windows (10 for the shipdeck investigation, 2 for the rotor inflow). The synchronisation of the two laser pulses with the image pair exposure was controlled by a six-channel Quantum Composer QC9618 pulse generator. A PIVpart30 particle generator by PIVTEC with Laskin atomizer nozzles was used for the seeding, which consisted of small oil droplets with diameters of 1-2 μm. The image pair analysis was carried out using PIVview 2C software[19]. The results that will be shown are the ensemble-averaged measurements over 800 image pairs. For the rotor inflow investigation, the closest points to the rotor plane (4.8 cm above the rotor

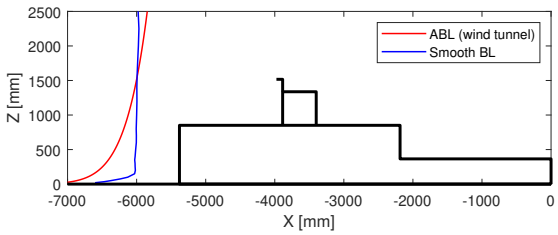

Figure 3: Adopted velocity profiles for the ABL reproduction with respect to the ship model. The position of the Pitot tube on top of the ship is shown.

hub centre) were extracted so that the normal induced velocity could be presented for a whole longitudinal diameter.

2.5. Atmospheric Boundary Layer Test Section

The tests were carried out in the large test chamber of the Large wind tunnel of Politecnico di Milano (GVPM[20]). The test chamber is 13.84 m wide, 3.84 m high and 38 m long. The test chamber is equipped with several devices allowing the production of different velocity profiles as well as different turbulence intensity and distributions. For the present activity, two different wind velocity profiles are considered: "Smooth flow", without any upstream turbulator, and "ABL", where turbulators were inserted upstream to obtain a velocity profile that corresponds to the well-known power law model:

$$\frac{U}{U_{REF}} = \left(\frac{Z}{Z_{REF}}\right)^{\alpha} \quad (2)$$

where α is an exponent that depends on the roughness of the terrain. The ABL velocity profile generated in this experiment corresponds to the wind profile with $\alpha = 0.1$ which is suggested By Simiu et al.[21] for coastal areas.

The two adopted velocity profiles for the ABL are shown in Figure 3 with respect to the ship model size. For further information about the features of the flow inside the test section, refer to Zasso et al.[22]. The velocity measured by a Pitot-Static probe placed above the ship superstructure was used as a reference velocity for setting the wind tunnel speed U_∞. This choice was driven by the fact that anemometers are usually placed close to that position in standard ships. In particular, for the actual test campaign, the Pitot measurement point was positioned 180 mm above and 90 mm upstream of the top superstructure, as shown in the sketch in Figure 3.

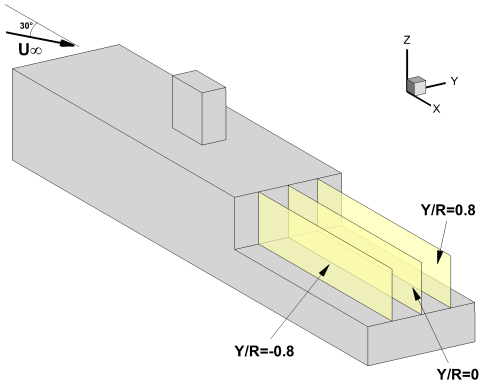

Figure 4: Position of the PIV investigation planes.

3. TEST POINTS AND LANDING TRAJECTORY

The experiments were conducted in two different test campaigns. The first campaign was focused on the qualification of the flow field on the flight deck without the helicopter model. Pressure measurements were made for all test points with and without presence of the ABL. For a selected number of tests, flow field visualization was made by means of PIV surveys in three longitudinal planes at different spanwise locations to cover the entire flight deck. Figure 4 shows the position of these measurement planes. To investigate the effect of the the wind velocity and direction, three advance ratios from three different directions were examined in the experiment. The advance ratios are corresponding to 20, 35 and 50 knots for the full scale model. Test parameters of the first campaign are summarized in Table 2.

During the second test campaign, to simulate the landing trajectory, the rotorcraft was positioned in a series of points representative of a typical stern landing trajectory. The trajectory, as shown in Figure 5, consists of five points (P1 to P5) that can be divided into two distinctive segments: the initial phase in which the helicopter approaches the flight deck from the stern side along the center line of the flight deck, followed by a descent phase, i.e. an oblique path towards the landing point, which is considered close to the center of the flight deck. Furthermore, three additional points above the landing point were selected to simulate a vertical descent (P5 to P8). Position of the rotor center for all test points is listed in Table 3 in which the height refers to the vertical offset with respect to the landing spot on the flight deck ($Z - Z_{DECK}$), and X is the distance from the stern of the ship. Due to

Table 2: Parameters of the first test campaign.

Test Number	Advance Ratio	Wind Direction	No. of PIV Plane3	Boundary Layer Type
1	0.0473	H	3	Smooth Flow/ABL
2	0.0828	H	0	Smooth Flow/ABL
3	0.1182	H	3	Smooth Flow/ABL
4	0.0473	R15	0	Smooth Flow/ABL
5	0.0828	R15	0	Smooth Flow/ABL
6	0.1180	R15	0	Smooth Flow/ABL
7	0.0473	R30	3	Smooth Flow/ABL
8	0.0828	R30	0	Smooth Flow/ABL
9	0.1182	R30	3	Smooth Flow/ABL

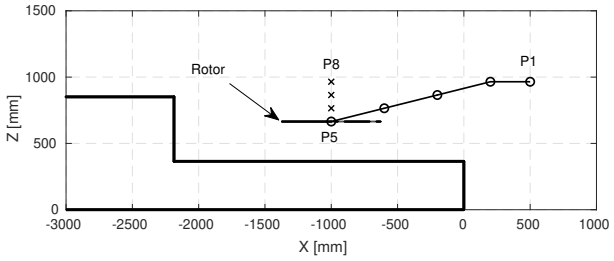

Figure 5: Side-view of landing trajectory. Circles and crosses represent the centre of the rotor for that particular test condition.

limitations of the current setup, the only PIV measures taken with the helicopter were at test points 1 and 7 of Table 2, both with the headwind and with R30 conditions at an advance ratio of $\mu = 0.0473$.

Table 3: Position of the rotor center

Test Point	Height [mm]	Height/R [-]	X [mm]
P1	600	1.6	500
P2	600	1.6	200
P3	500	1.3	-200
P4	400	1.07	-600
P5	300	0.8	-1000
P6	400	1.07	-1000
P7	500	1.3	-1000
P8	600	1.6	-1000
OGE	1135	3	700

4. RESULTS AND DISCUSSION

4.1. First Campaign: Ship Airwake Investigation

As previously stated, the first part of the test campaign was focused on the qualification of the flowfield on the flight deck without the helicopter. The regions of interest investigated by means of PIV was the flight deck, as represented in Figure 4. The main purpose of this investigation was to assess the influence of three parameters (presence of the ABL, wind speed, i.e. Reynolds number, and wind direction) on the flow structures above the shipdeck. Figures 6 and 7 present the comparison between the flow on the deck without (Smooth flow) and with (ABL) turbulator in terms of pressure and PIV measurements respectively. No significant difference between the two cases can be appreciated for both the pressure and the velocity field, hence implying that the ABL has not great influence on the flow developing on the shipdeck, at least for this scale of the adopted boundary layer velocity distribution. This was verified as well for a case at higher speeds (Test 3) and a case with wind coming from R30 (Test 7), which are not reported in the present paper for the sake of brevity.

The main flow differences were obviously found when changing the wind direction. In the headwind test condition, Figure 7, most of the air flowing on the shipdeck comes from above the hangar, creating a recirculation region past the vertical hangar wall. This flow topology is well known and is part of an arch vortex developing past a wall mounted obstacle[23], in this case the hangar.

Figure 8 presents the PIV measurements of Test 7 ($\beta = 30°$) with the isolated ship by means of contours of the in-plane velocity magnitude and streamlines, for the three selected longitudinal planes. $Y/R = -0.8$ corresponds to a plane close to the port side of the ship. In this plane, a recirculation region starts to develop close to edge of the hangar, while most of the shipdeck remains unaffected since in this region the air does not flow past the hangar step before arriving to the deck. Moving starboard, the recirculation region increases in size and thus the portion of the shipdeck interested by low-speed flow increases as well. Eventually, it can be appreciated for $Y/R = 0.8$, the most starboard investigation plane, the low-speed region covers almost entirely the deck.

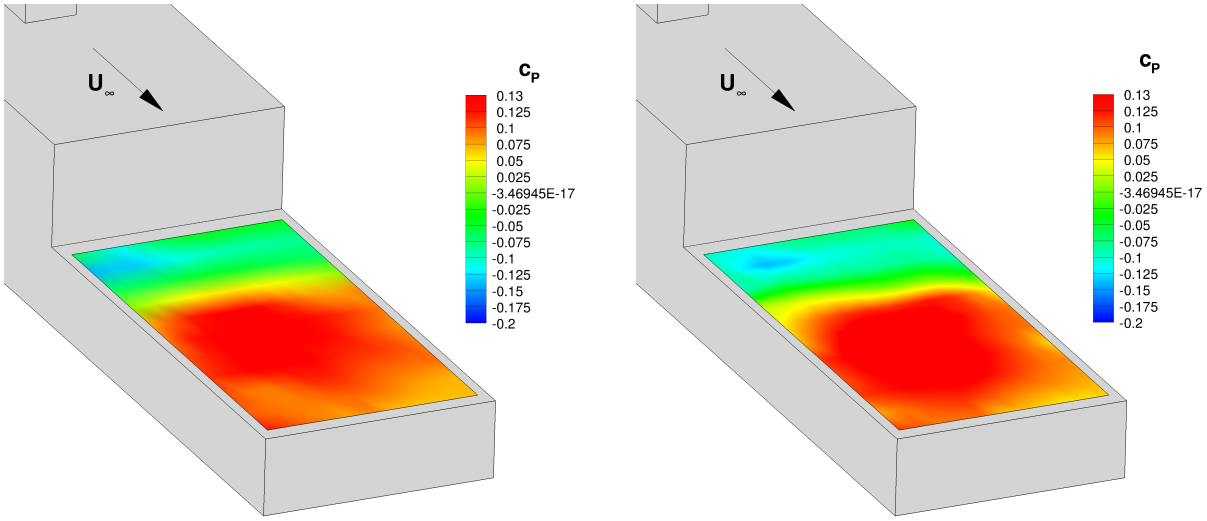

(a) Smooth flow (b) With ABL

Figure 6: Pressure coefficient contours of the isolated ship, comparison with and without ABL, U_∞=4.8 m/s $\beta = 0°$.

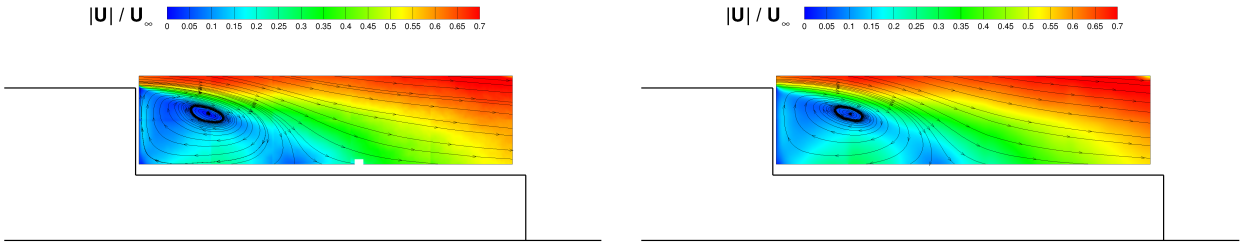

(a) Smooth Flow (b) With ABL

Figure 7: PIV measurements of the isolated ship. Contours of the in-plane velocity magnitude and streamlines in the symmetry plane ($Y/R = 0$), comparison with and without ABL, U_∞=4.8 m/s, $\beta = 0°$.

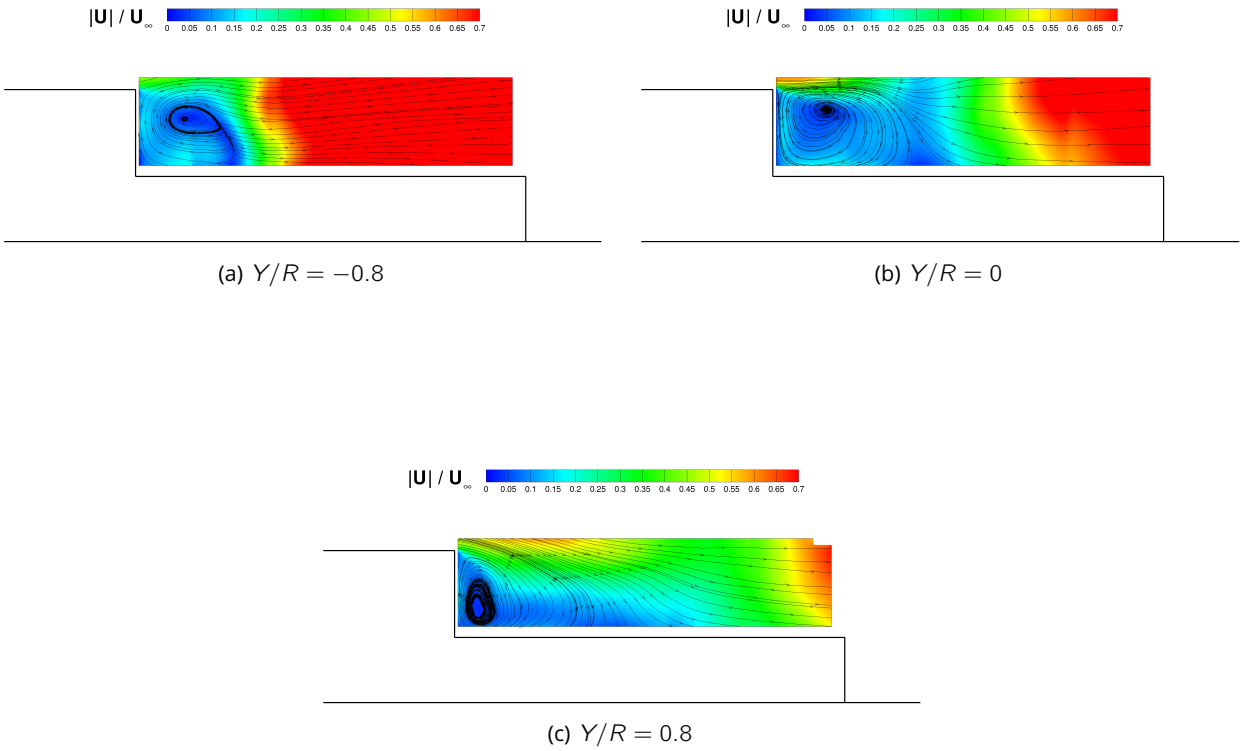

(a) $Y/R = -0.8$ (b) $Y/R = 0$

(c) $Y/R = 0.8$

Figure 8: PIV measurements of the isolated ship. Contours of the in-plane velocity magnitude and streamlines, for three different longitudinal planes, U_∞=4.8 m/s, $\beta = 30^\circ$.

4.2. Second Campaign: Helicopter-Ship Interaction

During the second test campaign, to simulate the landing trajectory, the rotorcraft was positioned in a series of points representative of a typical stern landing approach and then on a vertical descent. Load measurements on the rotor for the two approaches are shown in Figure 9, induced velocity profiles above the rotor are in Figures 10 and 11, while pressure contours on the shipdeck are shown in Figure 12.

Loads are expressed in terms of ratio with respect to the relevant out of ground effect (OGE) value in absence of the wind: hence thrust coefficient is divided by the OGE thrust coefficient, $c_{T,OGE} = 7.28 \times 10^{-3}$, whereas the in-plane moment coefficients were divided by the OGE torque coefficient, $c_{Q,OGE} = 7.74 \times 10^{-4}$. According to the load-cell axes, a positive pitch moment corresponds to a nose-down moment, and a positive roll moment promotes a rotation of the rotor thrust starboard.

Let us first focus on the stern landing without wind in the wind tunnel. Looking at the thrust coefficient plot of Figure 9(a), the typical thrust increase (up to 15%) due to ground effect can be seen as the helicopter gets closer to the landing spot ($X = -1000$ mm). The same behaviour can be appreciated for the vertical landing as well, as plotted in Figure 10(a) where a remarkable induced velocity reduction can be appreciated when the helicopter is moved from P8 to P5. However the ground effect experienced during the vertical landing is less intense with respect to the stern landing at the same heights. For instance, when the helicopter is placed in P6 ($X = -1000$ mm, $Z - Z_{DECK} = 400$ mm), the rotor experiences just a 8% thrust increase with respect to 10% of P4 ($X = -600$ mm, $Z - Z_{DECK} = 400$ mm), which is at the same height but further from the hangar vertical wall. This is caused by the the development of a recirculation region between the hangar wall and the helicopter. This recirculation consists of the rotor wake that, after being deflected by the shipdeck and by the hangar wall, is re-ingested by the rotor itself. This causes an increased induced velocity in the fore part of the rotor, together with the consequent thrust loss. A similar difference could be seen also between P3 and P7 measures that are both at the same height but different distance from the hangar wall.

The beneficial effects due to ground effect are mitigated in windy conditions, especially when the wind is blowing with a 30° angle with respect to the longitudinal ship axis, where a 10% thrust reduction can be seen when the helicopter is on the landing

spot (see Figure 9(a)). This can be also seen from the induced velocity plots of figure 11(a), where the classical induced velocity reduction due to ground effect on P5 is clearly mitigated when wind is blowing. This is even more accentuated during a vertical approach (see Figure 9(b)) at all points, and in particular at point P8 where values below the OGE thrust are reached.

Let us now consider the variation in the in-plane moment coefficients. The large moments registered far from the landing spot are consistent with the fact that the experiment was carried out with a rigid rotor without shaswplate and flapping hinges, hence it could not be trimmed in advanced flight. This is why we will now discuss the moments in terms of variations from the furthermost helicopter condition, the OGE condition.

Considering the in-plane moments, very limited moment variations are appreciated in absence of wind, for both the fore-aft and vertical approach. Larger variations were found in presence of wind, as the helicopter entered in the airwake developed by the ship. While the pitching moment trend during the fore-aft and vertical landing remains quite similar between the headwind and the R30 case, significant variations, up to 60%, can be appreciated for the roll moments. In particular, the roll moment remains negative and almost constant for the headwind case, whereas a strong decrease can be noted for the $\beta = 30^\circ$ case, starting from positive values towards an almost null value when the helicopter reaches the landing spot (P5).

To have a better understanding of the interacting flow field, let us consider the pressure contours. A comparison in the pressure coefficient between the headwind ($\beta = 0^\circ$) and R30° ($\beta = 30^\circ$) is shown in Figure 12, for three different positions of the helicopter. P5 ($X = -1000$ mm, $Z - Z_{DECK} = 300$), which corresponds to the landing spot, P4 ($X = -400$ mm, $Z - Z_{DECK} = 400$), which is a point on the oblique descending path and P8 ($X = -1000$ mm, $Z - Z_{DECK} = 600$), which is the highest point of the vertical path. Looking at the landing spot P5, Figure 12(a), a strong high-pressure region corresponding to the rotor wake impingement area is clearly visible in both cases, but a deeper low-pressure on the left portion of the obstacle can be appreciated for the $\beta = 30^\circ$ case owing to the wind blowing from the port side of the ship. c_P values higher than one are consistent with the pressures being non-dimensionalised using the wind dynamic pressure, since in the considered test conditions the rotor-induced velocity was higher than the asymptotic wind. The pressure contours remain qualitatively similar for the other two test points, but with lower pressure peaks in correspondence to the rotor wake impingement area, owing to the greater rotor distance with respect to the shipdeck.

5. CONCLUSIONS

In the present paper a wind tunnel investigation of a helicopter model in shipboard operations was presented. The ship was equipped with several pressure taps, while the forces on the rotor were monitored by means of a six-component load cell. Particle Image Velocimetry was used to investigate the flow on the shipdeck and the rotor inflow.

In the first phase of the experiment, the pressure and PIV survey of the flow field on the flight deck were performed without the presence of the helicopter, to study the flow features on the ship deck for several wind conditions, in particular to assess the influence of wind direction and of the Atmospheric Boundary Layer. Tests were carried out setting as wind velocity the one measured on a reference point by a Pitot-Static probe positioned on the ship superstructure. The presence of the Atmospheric Boundary Layer did not affect significantly the flow topology on the shipdeck, and this was verified for different wind intensities and directions.

Then, the rotorcraft was positioned in a series of points representative of a typical stern landing trajectory and a vertical descent. Typical ground effect thrust increase was appreciated for both landing trajectories, which appeared to be mitigated in presence of the wind. However, the influence of the ship airwake on the rotor inflow was not negligible for different rotor positions. When the wind was blowing from a 30° port direction, severe detrimental effects were encountered in terms of thrust loss, especially during the vertical trajectory. The pitch moment variations that were found when the helicopter entered in the ship airwake did not show a large dependance on the wind directions, in contrast to what occured to the roll moment.

ACKNOWLEDGMENTS

The NITROS (Network for Innovative Training on ROtorcraft Safety) project has received funding from the European Union's Horizon 2020 research and innovation program under the Marie Skłodowska-Curie grant agreement No. 721920.

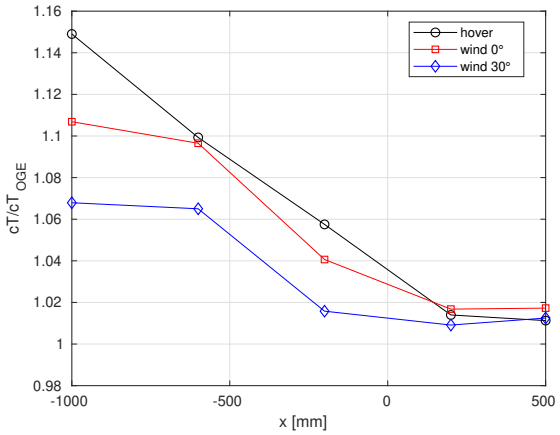

(a) Thrust coefficient, stern landing

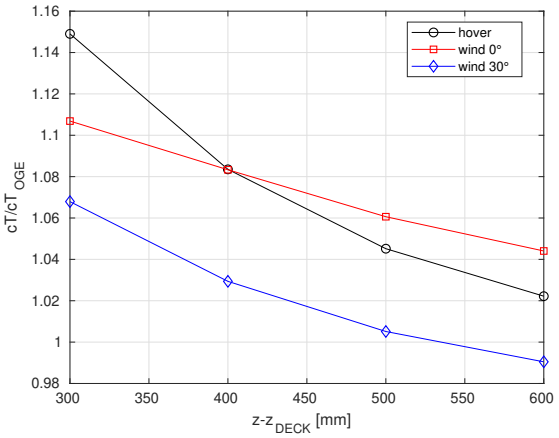

(b) Thrust coefficient, vertical landing

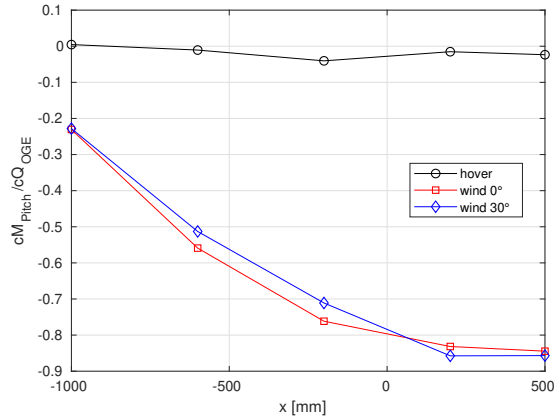

(c) Pitch moment coefficient, stern landing

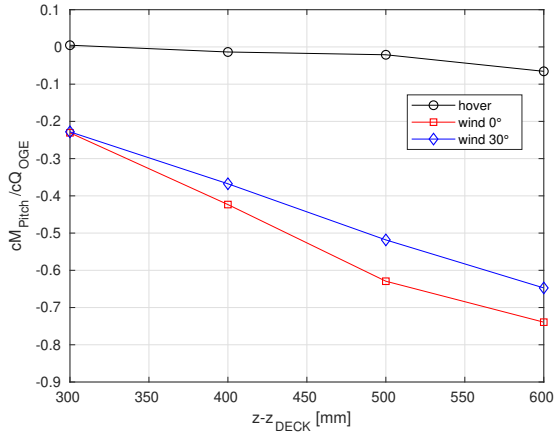

(d) Pitch moment coefficient, vertical landing

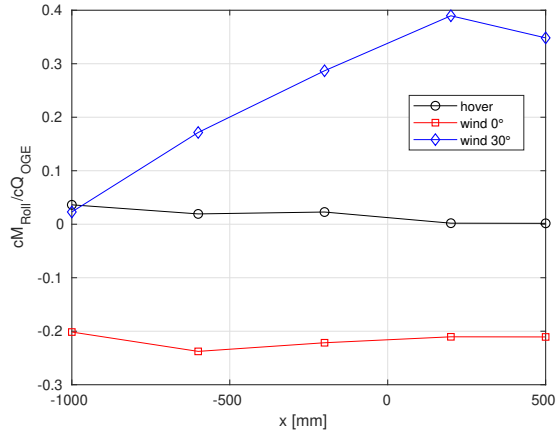

(e) Roll moment coefficient, stern landing

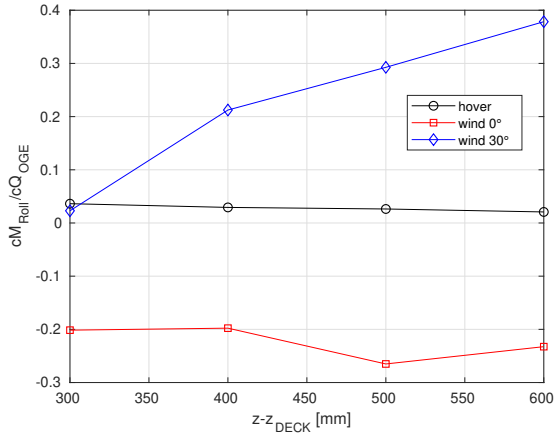

(f) Roll moment coefficient, vertical landing

Figure 9: Loads acting on the rotor. Comparison between stern approach (left) and vertical approach (right), for three different test conditions: wind-off case ("hover"), wind-on at $\mu = 0.0473$ and $\beta = 0°$. wind-on at $\mu = 0.0473$ and $\beta = 30°$.

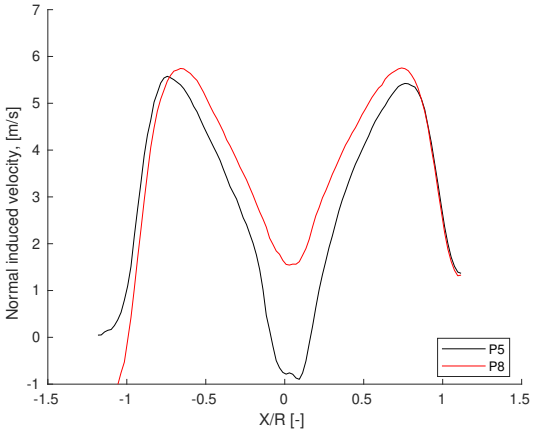

(a) Hover

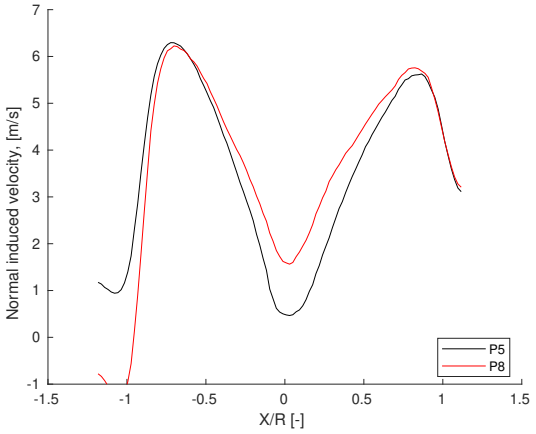

(b) Wind-on at $\mu = 0.0473$ and $\beta = 0^\circ$

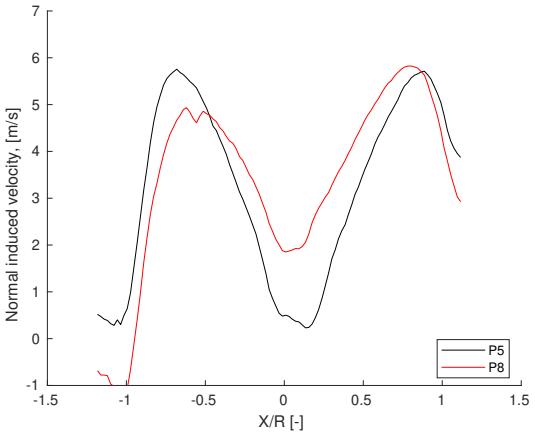

(c) Wind-on at $\mu = 0.0473$ and $\beta = 30^\circ$

Figure 10: Longitudinal induced velocity profiles on the rotor. Comparison for different rotor positions in different test conditions: wind-off case (a), wind-on at $\mu = 0.0473$ and $\beta = 0^\circ$ (b) and wind-on at $\mu = 0.0473$ and $\beta = 30^\circ$ (c).

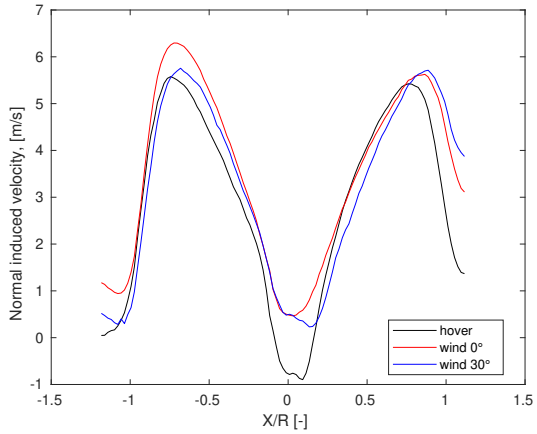

(a) P5

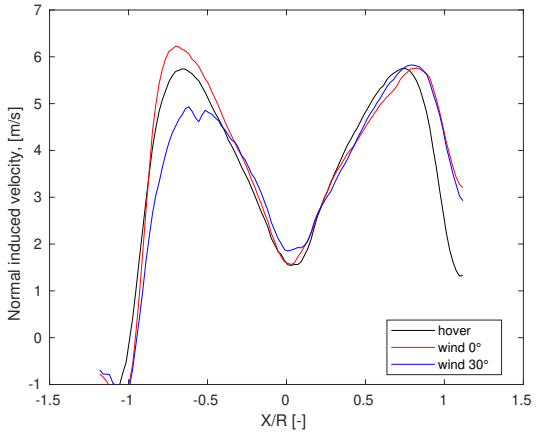

(b) P8

Figure 11: Longitudinal induced velocity profiles on the rotor. Comparison for in different test conditions in different rotor position: P5 (a), P8(b).

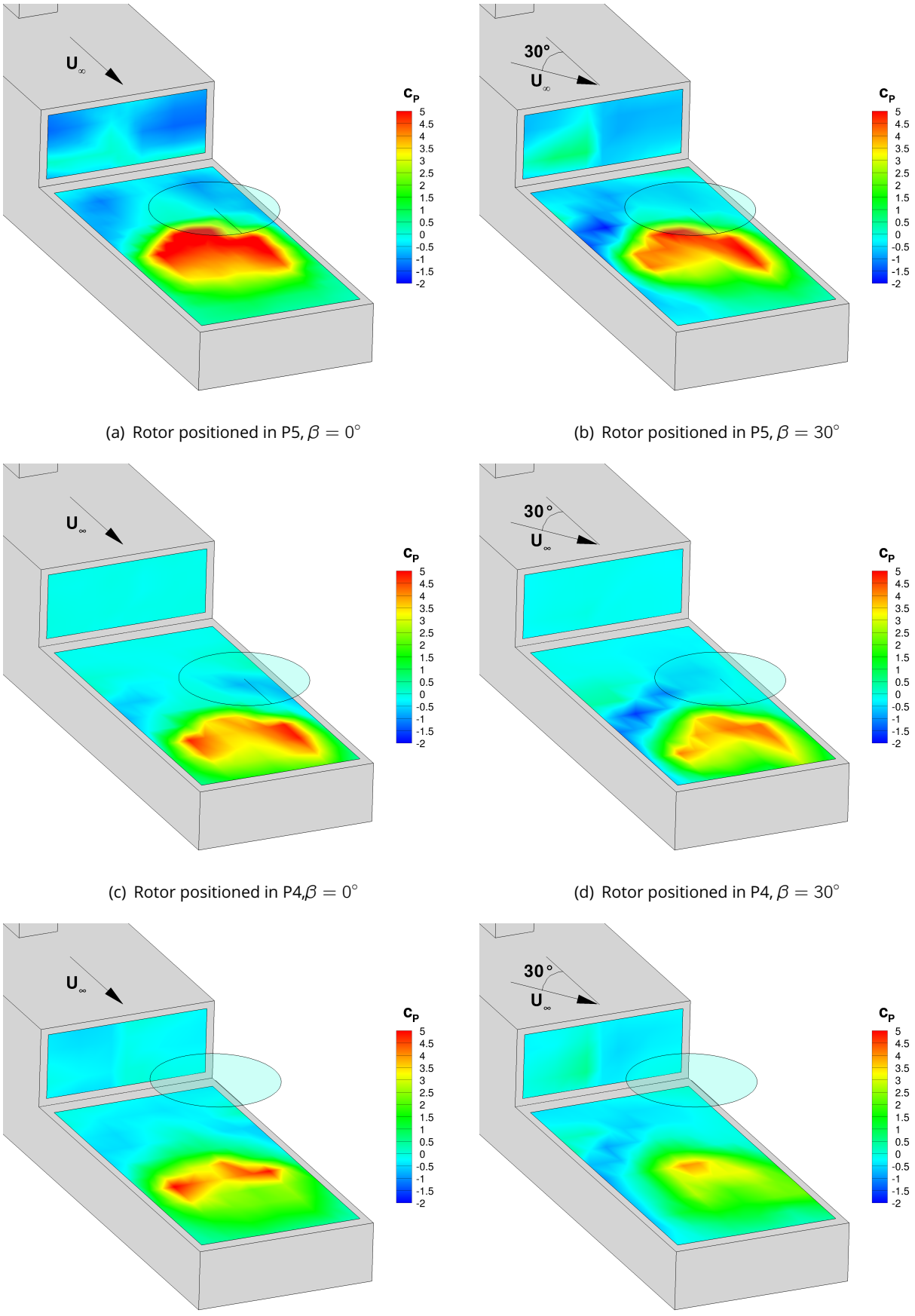

(a) Rotor positioned in P5, $\beta = 0^\circ$

(b) Rotor positioned in P5, $\beta = 30^\circ$

(c) Rotor positioned in P4,$\beta = 0^\circ$

(d) Rotor positioned in P4, $\beta = 30^\circ$

(e) Rotor positioned in P8, $\beta = 0^\circ$

(f) Rotor positioned in P8, $\beta = 30^\circ$

Figure 12: Pressure coefficient contours.

REFERENCES

[1] Garnett, T. and Davis, J., "The helicopter/ship dynamic-interface problem," Navy/NASA V/STOL Flying Qualities Workshop, 1977.

[2] Owen, I., White, M. D., Padfield, G. D., and Hodge, S. J., "A virtual engineering approach to the ship-helicopter dynamic interface a decade of modelling and simulation research at the University of Liverpool," *The Aeronautical Journal*, Vol. 121, (1198), 2013, pp. 1233–1248.

[3] Chirico, G., Szubert, D., Vigevano, L., and Barakos, G. N., "Numerical modelling of the aerodynamic interference between helicopter and ground obstacles," *CEAS Aeronautical Journal*, Vol. 8, (4), December 2017, pp. 589–611.

[4] Zan, S., "On aerodynamic modelling and simulation of the dynamic interface," *Proceedings of the Institution of Mechanical Engineers, Part G: Journal of Aerospace Engineering*, Vol. 219, (5), 2005, pp. 393–410.

[5] Quaranta, G., Barakos, G., Mulder, M., Pavel, M., and White, M., "NITROS an innovative training program to enhance rotorcraft safety," th AHS Forum, 2018.

[6] Zan, S. J., "Experimental determination of rotor thrust in a ship airwake," *Journal of the American Helicopter Society*, Vol. 47, (2), 2002, pp. 100–108.

[7] Lee, R. G. and Zan, S. J., "Wind tunnel testing of a helicopter fuselage and rotor in a ship airwake," *Journal of the American Helicopter Society*, Vol. 49, (2), 2004, pp. 149–159.

[8] Lee, R. G. and Zan, S. J., "Wind tunnel testing of a helicopter fuselage and rotor in a ship airwake," *Journal of the American Helicopter Society*, Vol. 50, (4), 2005, pp. 326–337.

[9] Kääriä, C. H., Wang, Y., Padfield, G. D., Forrest, J. S., and Owen, I., "Aerodynamic Loading Characteristics of a Model-Scale Helicopter in a Ship's Airwake," *Journal of Aircraft*, Vol. 49, (5), 2012, pp. 1271–1278.

[10] Kääriä, C. H., Wang, Y., White, M. D., and Owen, I., "An experimental technique for evaluating the aerodynamic impact of ship superstructures on helicopter operations," *Ocean Engineering*, Vol. 61, 2013, pp. 97–108.

[11] Nacakli, Y. and Landman, D., "Helicopter downwash/frigate airwake interaction flow-field PIV surveys in a low speed wind tunnel," American Helicopter Society 67th Annual Forum, Virginia Beach, VA, May 2011.

[12] Stargel, D. and Landman, D., "A Wind Tunnel Investigation of Ship Airwake/Rotor Downwash Coupling Using Design of Experiments Methodologies," 50th AIAA Aerospace Sciences Meeting, Nashville, Tennessee, Jan 2012.

[13] Quinliven, T. and Long, K., "Rotor performance in the wake of a large structure," American Helicopter Society 65th Annual Forum, Grapewine, TX, May 2009.

[14] Gibertini, G., Grassi, D., Parolini, C., Zagaglia, D., and Zanotti, A., "Experimental investigation on the aerodynamic interaction between a helicopter and ground obstacles," *Proceedings of the Institution of Mechanical Engineers, Part G: Journal of Aerospace Engineering*, Vol. 229, (8), 2015, pp. 1395–1406.

[15] Zagaglia, D., Zanotti, A., and Gibertini, G., "Analysis of the loads acting on the rotor of a helicopter model close to an obstacle in moderate windy conditions," *Aerospace Science and Technology*, Vol. 78, (8), 2018, pp. 580–592.

[16] Taymourtash, N., Zagaglia, D., Zanotti, A., Gibertini, G., and Quaranta, G., "Towards a Wind Tunnel Testing Environment for Rotorcraft Operations Close to Obstacles," 75th International Annual Forum American Helicopter Society (AHS), 2019.

[17] Reddy, K. R., Toffoletto, R., and Jones, K. R., "Numerical simulation of ship airwake," *Computers and fluids*, Vol. 29, (4), May 2000, pp. 451–465.

[18] Healey, J. V., "Establishing a database for flight in the wakes of superstructures," *Journal of Aircraft*, Vol. 29, (4), 1992, pp. 559–564.

[19] PIVTEC, *PIVview 2C version 3.0, User Manual*, available online at www.pivtec.com.

[20] Gibertini, G., Gasparini, L., and Zasso, A., "Aerodynamic design of a civil-aeronautical low speed large wind tunnel," AGARD 79th Fluid Dynamics Panel Symposium, 1997.

[21] Simiu, E. and Scanlan, R. H., *Wind Effect on Structures Fundamentals and Applications to Design*, John Wiley and Sons Inc., third edition, 1986, Chapter 2, p. 46.

[22] Zasso, A., Giappino, S., Muggiasca, S., and Rosa, L., "Optimization of the boundary layer characteristics simulated at Politecnico di Milano Boundary Layer Wind Tunnel in a wide scale ratio ranger," Proceedings of the 6th Asia-Pacific Conference on Wind Engineering, 2005.

[23] Martinuzzi, R., Tropea, C., *et al.*, "The flow around surface-mounted, prismatic obstacles placed in a fully developed channel flow," *Transactions-American Society of Mechanical Engineers Journal of Fluids Engineering*, Vol. 115, 1993, pp. 85–85.